ADVANCED FUNCTIONAL MATERIALS
www.afm-journal.de

Materials Views
www.MaterialsViews.com

Synchrotron X-Ray Scanning Tunneling Microscopy: Fingerprinting Near to Far Field Transitions on Cu(111) Induced by Synchrotron Radiation

Volker Rose, Kangkang Wang, TeYu Chien, Jon Hiller, Daniel Rosenmann, John W. Freeland, Curt Preissner, and Saw-Wai Hla*

The combination of the high spatial resolution of scanning tunneling microscopy with the chemical and magnetic contrast provided by synchrotron X-rays has the potential to allow a unique characterization of advanced functional materials. While the scanning probe provides the high spatial resolution, synchrotron X-rays that produce photo-excitations of core electrons add chemical and magnetic contrast. However, in order to realize the method's full potential it is essential to maintain tunneling conditions, even while high brilliance X-rays irradiate the sample surface. Different from conventional scanning tunneling microscopy, X-rays can cause a transition of the tip out of the tunneling regime. Monitoring the reaction of the z-piezo (the element that controls the tip to sample separation) alone is not sufficient, because a continuous tip current is obtained. As a solution, an unambiguous and direct way of fingerprinting such near to far field transitions of the tip that relies on the simultaneous analysis of the X-ray-induced tip and sample current is presented. This result is of considerable importance because it opens the path to the ultimate resolution in X-ray enhanced scanning tunneling microscopy.

1. Introduction

The ability to directly obtain electronic, chemical, and magnetic information of materials at the nanoscale is of tremendous importance for the progress in nanoscience and nanotechnology. Scanning tunneling microscopy (STM) has become an indispensable tool for the understanding of structural and electronic properties of nanoscale systems down to the atomic scale.[1,2] The high spatial resolution of STM is made possible by the exponential dependence of the tunneling current from the tip/sample separation. However, despite its indisputable success STM lacks the capability of direct chemical or elemental contrast. Only in very specific cases do various effects lead to indirect chemical contrast.[3–5] The lack of direct chemical contrast is due to the fact that tunneling electrons originate only from states close to Fermi energy. Unfortunately, these states do not carry any direct elemental specificity. In contrast, core electrons maintain their chemical fingerprint even in bulk materials, but their probability for tunneling is negligible. Thus, the excitation of core electrons to unoccupied levels close to the Fermi energy that contribute to the tunnel current would open a path to high-resolution microscopy with chemical contrast. Synchrotron X-ray scanning tunneling microscopy (SXSTM) has the potential to meet this goal (**Figure 1**).[6] This technique combines the high spatial resolution of STM with the electronic, chemical, and magnetic sensitivity of synchrotron X-rays. While the tip is rastering across the surface, absorption of photons by the sample can excite electrons to unoccupied levels close to the Fermi energy. At the same time photoelectrons are ejected from the sample.[7] The conducting tip that is tunneling over a sample surface can locally measure these excited electrons. Additionally, magnetic contrast can be obtained due to the dependence of photoabsorption by a magnetic material on the helicity of the X-rays.[8,9] In recent years, the high prospects of combining scanning tunneling microscopy and other scanning probe variants with synchrotron radiation has generated multifaceted promising research.[10–15] Chemical contrast with a spatial resolution of about 10 nm has already been reported.[16,17] It is expected that the spatial resolution can be further enhanced by means of special insulator coated tips with a minimized conducting apex, which avoid the exposure of the sidewall of the tip to photoejected electrons.[18–20] However, to achieve ultimate resolution it will be critical to maintain stable tunneling conditions during X-ray excitation.

Dr. V. Rose
Advanced Photon Source & Center for Nanoscale Materials
Argonne National Laboratory
9700 South Cass Avenue
Argonne, IL 60439, USA
E-mail: vrose@anl.gov
Dr. K. K. Wang, D. Rosenmann, Dr. S.-W. Hla
Center for Nanoscale Materials
Argonne National Laboratory
9700 South Cass Avenue, Argonne, IL 60439, USA
J. Hiller
Electron Microscopy Center
Argonne National Laboratory
9700 South Cass Avenue, Argonne, IL 60439, USA
Dr. T. Chien, Dr. J. W. Freeland, Dr. C. Preissner
Advanced Photon Source
Argonne National Laboratory
9700 South Cass Avenue, Argonne, IL 60439, USA

DOI: 10.1002/adfm.201203431

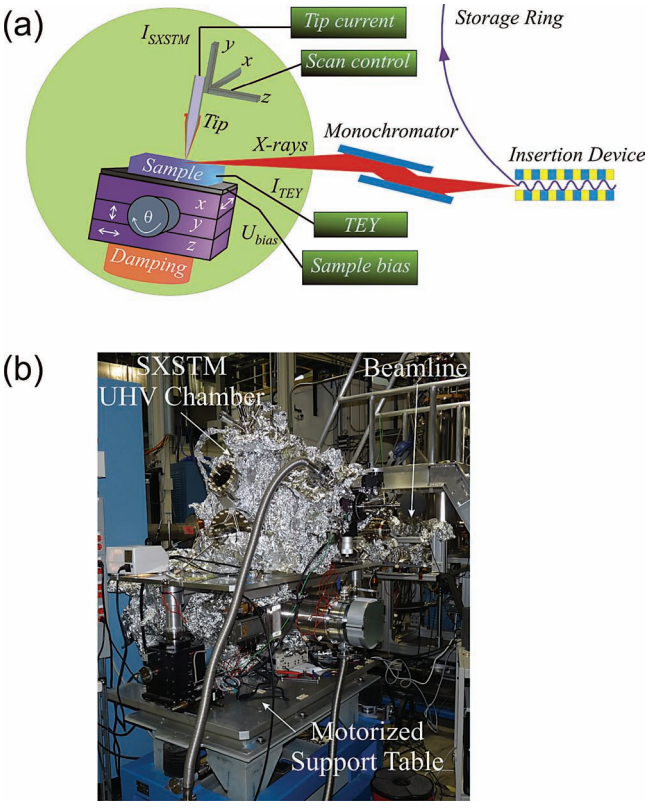

Figure 1. a) Schematic representation of SXSTM. An insertion device at the synchrotron storage ring serves as X-ray source for the experiment. The photon energy can be selected by a monochromator. Rotational (θ) and translational (x, y, z) degrees of freedom are available at both the sample and the tip. A damping stage provides vibration isolation of the microscope. Tip and sample current are recorded simultaneously. b) The SXSTM system at the synchrotron beamline 4-ID-C of the Advanced Photon Source, Argonne National Laboratory.

In this paper, we used a specially fabricated STM tip to directly determine the tip transitions from tunneling (near field) into the far field. This important observation should be used to revisit past research in the field, because a transitions might not always be obvious in SXSTM images due to the continuous nature of the detected current. Controlling the near to far field transition will open the path to high-resolution characterization of advanced materials, in which chemical variations at the nanoscale determine properties of functional materials. Additionally, our results allow separating the actual amounts of X-ray induced tunneling and photoejected currents when the tip is tunneling over the sample surface.

2. Results and Discussion

In SXSTM, a synchrotron X-ray beam illuminates the sample surface at an area of typically tens of microns. Thus, for locally resolved measurements of X-ray induced currents at the tip-sample junction, the number of photoelectrons arriving at the sidewall of the tip needs to be reduced. One way to achieve this is by covering most of the tip with an insulating layer, which prevents detection of photocurrent at the sidewall of the tip. For this we used micro-fabricated SXSTM tips. **Figure 2** shows a scanning electron micrograph of a PtIr tip, which is entirely coated by a 500-nm-thick insulating SiO_2 film except at the apex. The coated tip with sub-micron conducting apex was prepared by means of electron beam physical vapor deposition, focused ion beam milling, and subsequent ion beam stimulated oxide growth.[20] The coating confines the detection of photoejected electrons to a small area at the tip apex. Like in any conventional STM measurement, the detection of a tunnel current is also restricted to the tip apex.

The near field tip current I_{SXSTM}^{tip} in SXSTM is caused by two components: tunneling and photoejected electrons. When a sample is illuminated with X-rays, the conventional tunnel current I_{tunnel}^{STM} experiences a modulation due to an absorption-induced tunnel current $I_{excited}^{X-ray}$, and contributions caused by photocurrents.[6] Electrons that are photoejected from the sample and are detected at the tip cause a current I_{pass}^{sample}, while the remaining electrons that escape without detection carry a current I_{loss}^{sample} away. At the same time currents I_{pass}^{tip} and I_{loss}^{tip} are generated at the tip, which describe electrons that leave the tip and reach the sample, or electrons that escape into the continuum without detection at the sample, respectively. Generally, the number of electrons that are excited to unoccupied levels close to Fermi energy E_F as well as photoejected electrons exhibits a sharp jump when the photon energy reaches one of the inner-shell ionization energies. This accounts for the chemical sensitivity in the tunneling as well as in the photoejected channel. In case of a positively biased sample the resulting signal at the tip is

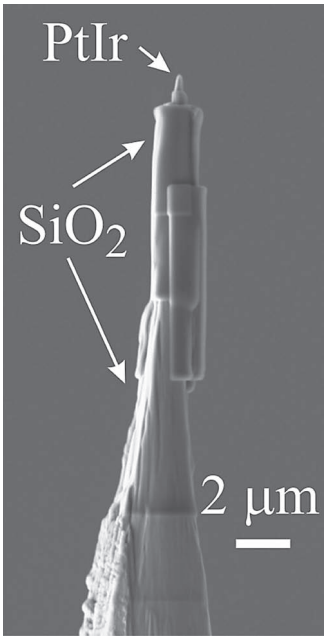

Figure 2. Scanning electron micrograph of the SiO_2-coated PtIr tip. The PtIr tip is only exposed over a length smaller than 0.5 µm.

$$I_{SXSTM}^{tip} = I_{pass}^{tip} + I_{loss}^{tip} - I_{pass}^{sample} + I_{tunnel}^{STM} - I_{excited}^{X-ray} \quad (1)$$

Likewise, a sample current $I_{\mathrm{SXSTM}}^{\mathrm{sample}}$ can be measured simultaneously.

$$I_{SXSTM}^{sample} = -I_{pass}^{tip} + I_{loss}^{sample} + I_{pass}^{sample} - I_{tunnel}^{STM} + I_{excited}^{X-ray} \quad (2)$$

In this convention, currents that arrive at the tip or sample are counted as negative, while currents that leave the tip or sample have a positive sign. The contribution $I_{\mathrm{excited}}^{\mathrm{X-ray}}$ denotes the reduction of tunnel current caused by the excitation of electrons into unoccupied sample states close to the E_F. For a negatively biased sample this contribution is an actual X-ray excited current that increases the conventional tunnel current. After electrons are ejected from either the sample or the tip they are accelerated in the electric field generated by the bias voltage between tip and sample. If the sample is positively biased photoelectrons are more likely to be recollected by the sample, because the negative potential of the tip repels those photoelectrons. The situation is reversed when the sample is negatively biased. Thus, the polarity and the size of the bias voltage allow an effective control over the photoelectron collection at the tip.

2.1. Spectroscopy with the Tip in the Far Field

In a first step, we have evaluated photo-excitations in a Cu(111) single crystal with the tip in the far field (≈180 nm tip/sample separation) where quantum mechanical tunneling does not take place. Thus, in this regime, the SXSTM tip is used just as a detector for the photoelectrons that are ejected from the sample surface and produce a photocurrent. During the measurement, the X-ray energy is ramped from 925 to 965 eV, a range that covers Cu L edge excitations. The SXSTM tip and the sample simultaneously detect the corresponding photocurrent. The data are recorded at different fixed sample voltages between ±5 V. Since this measurement set-up is not in the tunneling regime, the sample voltage just helps in reducing or enhancing the photocurrent depending on the bias polarity. **Figure 3** presents sample and tip current spectra obtained for X-ray energies close to the Cu L absorption edges as a function of applied bias between the grounded tip and the sample. The total electron yield (TEY) shown in Figure 3a was measured directly from the sample via the sample current method. The measured photocurrent range is in between 0.5 to 6.5 nA, and two pronounced peaks are observed at 932.5 and 952.5 eV, which represent the L_3 edge ($2p_{3/2}$ to 3d transition) and L_2 edge ($2p_{1/2}$ to 3d transition), respectively. The main peaks are accompanied by a series of smaller peaks at 936.4, 940.1, 956.3, and 960.5 eV, which indicate the presence of copper oxide.[21] All peaks are superimposed on a monotonically increasing background current generated by the continuum of photoejected electrons. The intensity of the Cu L peaks increases for more negative biases due to the larger electric field that repels ejected electrons from the sample surface.

The photocurrent arriving at the tip is also simultaneously recorded. Figure 3b shows the corresponding tip current spectra measured in the far field. Electrons that arrive at the tip give rise to a negative current.[22] Thus, negative peaks are observed in the tip current when the X-ray energy approaches the Cu L absorption edges. The detected tip current range is in between +0.01 to −0.34 nA, which is about 20 times smaller than the sample current at this tip-sample distance of 180 nm. Like in the case of the sample current, both the absolute value of the intensity of the Cu L peaks as well as the off-resonant tip current increase with more negative bias. Interestingly, for a bias of +3 V and above the tip current is positive for at least a portion of the spectrum. The change of the sign in the tip current can be explained when the total sum of ejected electrons is considered. The X-ray beam always simultaneously illuminates the sample surface and the tip thereby causing electron ejection from both. In the case of a positive tip current more electrons are ejected from the tip than arrive from the sample. On the other hand, a negative tip current can be observed when the number of electrons arriving from the sample is larger than the number of electrons leaving the tip.

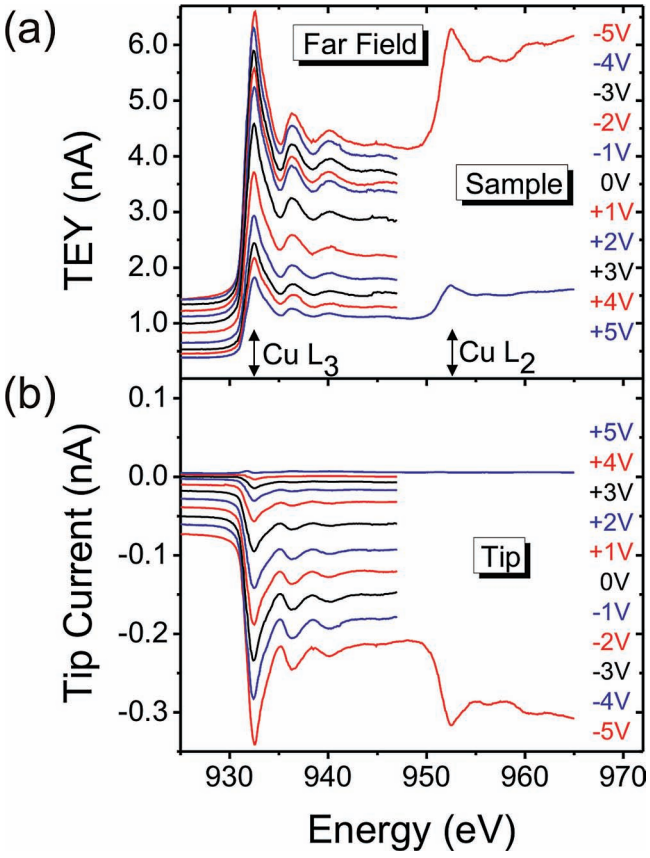

Figure 3. Spectroscopy with the tip located in the far field for biases from −5 to 5 V. a) The total electron yield (TEY) of the Cu(111) sample increases for more negative sample bias. b) The tip current exhibits negative peaks caused by the Cu L absorption edges.

The dependence of the tip current as a function of TEY is presented in **Figure 4**. In the far field, plotting the tip current as a function of TEY results in straight lines with characteristic slopes that are bias dependent. Negative slopes are observed for bias voltages between −5 and +4 V, but they turn to a positive

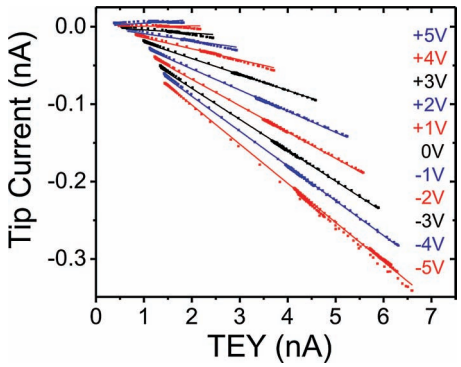

Figure 4. In the far field the tip current is directly proportional to the TEY with a slope that is characteristic for the applied bias. The straight lines are linear fits of the data points for each sample bias.

slope for a bias greater than 4 V. Generally, most ejected electrons are generated by secondary excitations and therefore have relatively low energy. Thus, these photoelectrons can be easily controlled by a small external field, which explains the strong bias dependence observed here. At 5 V, ejected electrons from the sample are effectively repelled from the tip.

2.2. Spectroscopy with the Tip Stabilized Under Tunneling Conditions

Next, we investigate the influence of synchrotron X-rays on the tip current in the near field. The tip is first stabilized in the tunneling regime without the X-ray beam at a current set point of 0.05 nA. At this point, the tip-sample distance should be about 1 nm or less. Then the X-ray shutter is opened and the X-ray energy is ramped from 925 to 947 eV, which covers the Cu L_3 adsorption edge. The corresponding tip and sample currents are recorded with the sample bias between ±3 V, which is the most relevant bias range utilized in conventional STM studies. **Figure 5**a presents the measured TEY after the tip was stabilized in the near field. The TEY varies between 0.5 to 6 nA. This measured current range is similar to the previous far field case between ±3 V (Figure 3a). Here, a peak at the Cu L_3 edge can be observed at 932.5 eV, and the intensity of this peak increases for more negative biases. While the spectra for −3 and −2 V are very smooth like far field spectra (c.f., Figure 3a), the other spectra appear to be noisy for photon energies in the pre-edge region (925–931 eV). Additionally, the spectra for 1 to 3 V are also noisy in the post-edge region (936–947 eV). As can be seen in the following, a smooth TEY is correlated with far field behavior, while the noisy characteristic is a consequence of electron tunneling.

The corresponding tip current is presented Figure 5b. For negative bias voltages of −3 and −2 V the tip current spectra are similar to the data obtained in the far field (see Figure 3b), with the current ranging from about −0.05 nA to −0.25 nA for minimum to maximum, respectively. The recorded current range is the same as in the far field regime measured previously, where the tip sample distance is about 180 nm. This indicates that for these negative biases the tip spontaneously leaves

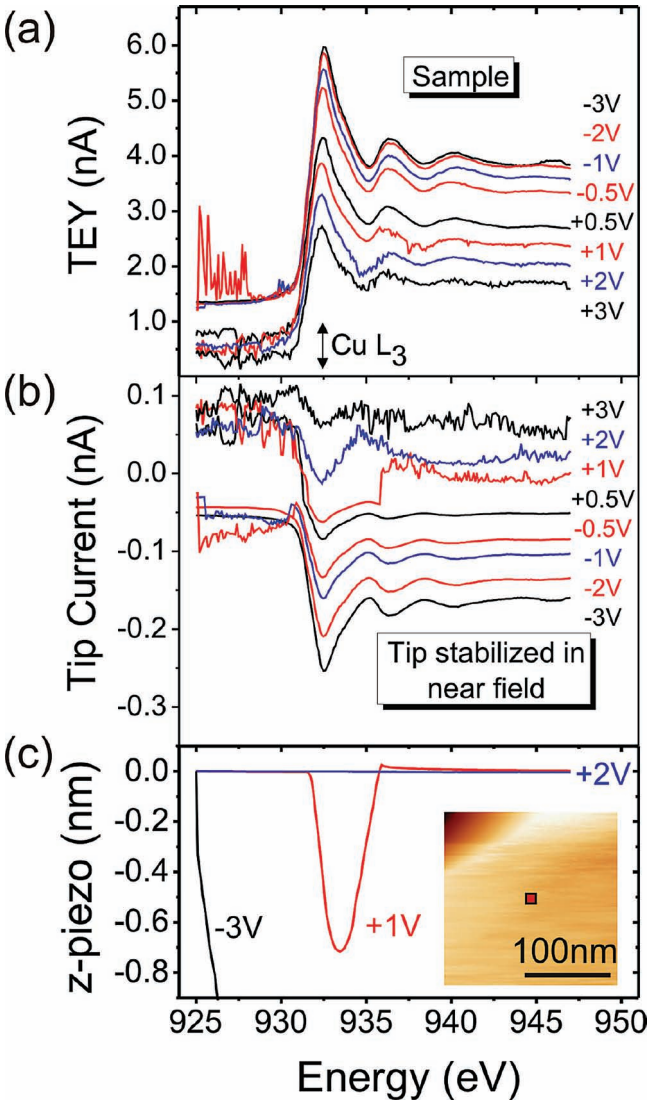

Figure 5. Spectroscopy after the tip was brought into tunneling over the sample surface, i.e., near field. The tip was stabilized at ±0.05 nA before the X-ray shutter was opened. a) Current measured at the sample (TEY) as a function of X-ray energy for biases between −3 and 3 V. (b) The corresponding tip current shows negative peaks at the Cu L_3 absorption edge. c) Reaction of the z-piezo relative to the stable tunneling condition without beam shown for selected bias voltages of −3, 1, and 2 V. The inset shows the Cu(111) surface with the location that was used for the spectroscopy (red square).

the tunneling regime during the energy ramp to move into the far field, because the current produced by the arriving electrons at the tip is larger than the setpoint value. However, between −1 V and +1 V the tip current spectra exhibit the noisy characteristic in the pre-edge region that has likewise been observed in the TEY spectra. Electron tunneling inherently causes the noisy characteristic, because of the strong exponential dependence of the tunneling current from the tip-sample separation. Around the Cu L_3 edge the spectra then transform into a smooth curves, which is caused by the transition of the tip into the far field (see Figure 3b). In the case of +1 V the spectrum

returns to a noisy characteristic for photon energies larger than 936 eV, i.e., the tip moves back into tunneling. The spectra measured at the positive biases of 2 and 3 V are significantly different. They show a noisy characteristic throughout the whole energy range. The tip remains in tunneling conditions during the whole energy ramp. Generally, in all scans the noisy and smooth regimes in the tip current and TEY spectra are directly correlated. These measurements provide important information: 1) although the tip was initially stabilized in the near field, i.e., tunneling, X-ray induced current can force the STM feedback to adjust the *z*-piezo in a way that the tip moves into the far field in order to maintain the current setpoint. 2) The tip current is continuous when the tip moves out of the tunneling regime, which makes the observation of such transitions difficult in conventional imaging. 3) The tip maintains tunneling conditions during the full energy scan for positive voltages of 2 V and above. Thus, at these bias voltages, the chemical contrast of the sample is achievable even during tunneling.

In order to understand the observed transitions in the spectra we investigate the reaction of the *z*-piezo as a function of X-ray energy. In Figure 5c, we present the response of the *z*-piezo for applied biases of –3, +1, and +2 V, respectively. The height of the *z*-piezo is shown relative to the stable tunneling condition without the X-ray beam. In the case of +2 V bias, the *z*-piezo does not exhibit a response to the X-ray illumination of the sample. In contrast, at +1 V the tip retracts by about 0.7 nm when the X-ray energy approaches the Cu L_3 edge. This response is directly correlated to the transition from positive to negative current (see Figure 5b). The reaction of the *z*-piezo is even more pronounced at –3 V. Here, the tip retracts immediately after the X-rays start to illuminate the sample surface even before the Cu L_3 energy is reached. This *z*-piezo response results in a negative tip current spectrum like in the far field regime.

The display of the tip current as a function of TEY in **Figure 6** demonstrates that the *z*-piezo response and the tip current spectra are directly related to transitions of the tip from the near field (tunneling) into the far field (no tunneling), and under certain conditions even back to the near field. In the case of a bias of –3 V all data points lie on a straight line with a slope that coincides with the one observed for the tip in the far field (see Figure 4). This indicates that the tip immediately moves into the far field as soon as X-rays illuminate the sample in negative biases. Generally, the tip current in SXSTM consists of two components: tunneling current and the current produced by photoejected electrons. If the sum of these currents exceeds the current setpoint for standard tunneling, the *z*-piezo will react in order to maintain the predetermined setpoint. However, considerably different from conventional STM the collapse of electron tunneling will not yield zero tip current. In SXSTM we rather measure a continuous tip current even during transitions between near and far field. Most likely this explains the poor image quality of several SXSTM images presented in the literature. Transitions can also be reversible. At a bias of 1 V, the tip experiences a transition from tunneling into the far field and back into tunneling (arrows in Figure 6). Stable tunneling conditions are preserved for bias voltages of 2 V and above. In this case, the data points do not approach the corresponding far field slope (dashed line in Figure 6). Thus, the observation

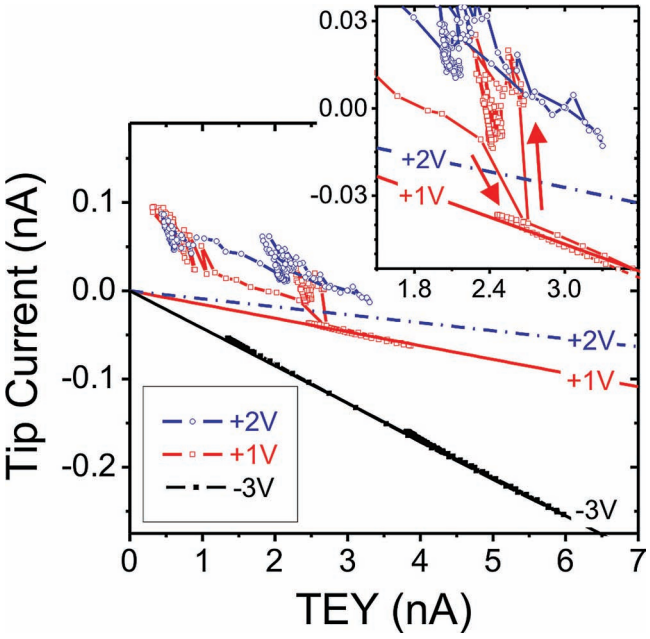

Figure 6. Tip current as a function of TEY. For a bias of –3 V all data points lie on the linear slope, which is characteristic for the tip in the far field. A transition to and from a linear slope is observable for 1 V (inset). At a bias of 2 V the data points never approach the expected linear slope (dashed line).

of the tip current as a function of TEY provides a direct fingerprinting of near to far field transitions in SXSTM.

2.3. Quantification of X-Ray-Induced Currents During Tunneling

Measurements in the far field allow studying the photoejected electrons. In the far field the terms in Equation 1 that are associated with tunneling vanish, and a tip current

$$I_{SXSTM}^{tip} = I_{pass}^{tip} + I_{loss}^{tip} - I_{pass}^{sample} \quad (3)$$

is obtained.

However, in the near field both tunneling and photoejection will simultaneously contribute to the current. Therefore, it is difficult to determine the individual current contributions in Equation 1 as long as the tip stays in tunneling conditions. Nevertheless, we will show that the different contributions to the tip current in the near field can be entangled using the measured spectra for the bias voltage of 2 V. For this bias, the tip maintains tunneling conditions during the whole energy scan. At the Cu L_3 edge, the tip current in the near field $I_{SXSTM}{}^{tip}$ amounts to –12.9 pA (Figure 5b). For the same bias $I_{SXSTM}{}^{tip}$ = –30.3 pA is measured in the far field (Figure 3b).

It is possible to extrapolate the measured current values at 180 nm separations into the tunneling regime. **Figure 7** shows a measurement of the tip current as a function of *z*-piezo positions. Here, the tip was first stabilized at a current setpoint of –0.375 nA, a bias voltage of –2 V, and a photon energy of 932.5 eV. Subsequently, the vertical tip position was ramped

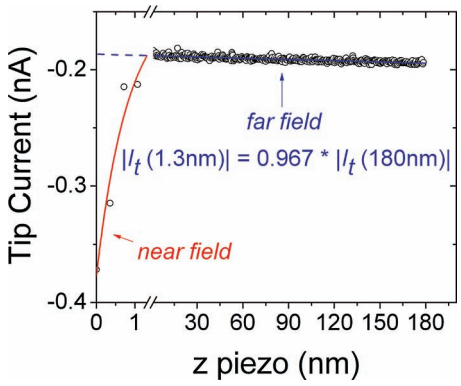

Figure 7. Tip current as a function of tip/sample separation. The tip was stabilized at –0.375 nA, –2 V, 932.5 eV, and then ramped away from the surface while the tip current was recorded. The exponential behavior in the near field (0–1.3 nm) is caused by the exponential dependence of the tunneling current as a function of the tip/sample separation. After the tip leaves the tunneling regime the current only slightly depends on the distance. This allows extrapolating the current contribution of photoejected electrons into the near field.

away from the surface, while simultaneously the corresponding tip current was recorded. The current exhibits an exponential dependence in the near field (0 to about 1.3 nm). This is a consequence of the exponential dependence of the tunnel current with respect to the tip/sample distance. After the tip leaves the near field the tip current remains almost constant up to the measured separation of 180 nm. The small increase in the absolute value of the tip current is caused by a geometrical effect.[7] More ejected electrons are able to reach the tip apex when it is further away from the sample surface. About 96.7% of the measured tip current at 180 nm is detected at 1.3 nm separation. The linear behavior allows extrapolating the measured far field currents into the tunneling regime. Hence, in the case of the bias voltage of 2 V, a photoejected current $I_{pass}^{tip} + I_{loss}^{tip} - I_{pass}^{sample}$ of –29.3 pA is present in the tunneling regime. The conventional tunnel current I_{tunnel}^{STM} amounts to 50 pA, which is the initial current setpoint that was used to stabilize the tip. This term is constant throughout the scan because the height of the tip does not change (c.f., Figure 5c). Using Equation 1, we can calculate $I_{excited}^{X\text{-}ray} = 33.6$ pA, which is caused by X-ray induced excitations of electrons to unoccupied levels close to E_F in the sample. These excited electrons will reduce the number of available states for electrons that try to tunnel from the tip into the sample. Hence, this leads to a virtual current with a positive sign.

The photoejected current can be further analyzed. During the initial alignment of the synchrotron beam the X-rays only illuminate the apex of the tip. This allows measuring the photoejection from the tip. Here, the sum $I_{pass}^{tip} + I_{loss}^{tip}$ amounts to 15 pA. After the alignment the sample is moved toward the tip, which maintains the alignment of the tip apex in respect to the stationary X-ray beam. Consequently, during tunneling the ejected electrons from the sample that reach the tip, I_{pass}^{sample}, account for a current of 44.3 pA at the Cu L_3 edge. Generally, the chemical contrast at the Cu L_3 is achieved by both channels, $I_{excited}^{X-ray} = 33.6$ pA and $I_{pass}^{sample} = 44.3$ pA. This is an important result, because it proves that the tunneling channel is of the same order than the photoejected channel. It is well known that conventional STM can provide atomic resolution; thus, a comparable resolution in SXSTM is foreseeable. The ratio between tunneling and photoejection might be even further improved in the future with advances in the fabrication of insulator-coated smart tips with nanoscale exposed apex.[20]

3. Conclusions

We have utilized X-ray spectroscopy with the tip of an STM to detect transitions between near field and far field conditions caused by excitations mediated by synchrotron radiation. A characteristic feature of the tip in the far field is a linear dependence of the tip current as a function of the TEY. This dependence allows direct observation of the transition between near and far field. Thus, it is absolutely critical to simultaneously record both the tip and the sample current. Utilizing an insulator-coated tip we have found stable tunneling conditions on Cu(111) for a bias voltage of 2 or 3 V (0.05 nA setpoint). The observation of near to far field transitions is of particular importance, because these might not be directly obvious in tip current images because of the continuous nature of the detected current—only the comparison to the sample current can reveal that a near-to-far transition has occurred. Our measurements also reveal that chemical contrast within the tunneling condition is possible to achieve for a certain positive biases. At a bias voltage of 2 V, the chemical contrast has about the same magnitude in the tunneling and the photoejected channel. Taking advantage of findings presented in this work SXSTM has proven further to have the potential for providing ultra-high spatial resolution with chemical, electronic, and magnetic contrast of complex materials.

4. Experimental Section

Synchrotron Beamline: The experiments were performed at the soft X-ray beamline 4-ID-C of the Advanced Photon Source at Argonne National Laboratory.[23] The X-ray source on this beamline is a unique electromagnetic undulator capable of delivering both vertical and horizontal linear as well as circular polarization over the spectral range of 500 to 2800 eV. A spherical grating monochromator provides an energy resolution ($\Delta E/E$) of 2×10^{-4}. The focused X-ray beam with a nominal size of about 100×100 μm^2 exhibits at a photon flux of about 8×10^{11} photons/s.

Synchrotron X-Ray Scanning Tunneling Microscope: The STM is located inside of a dedicated ultra-high vacuum endstation that allows both in situ sample preparation and imaging. A spring suspension stage with eddy current damping is utilized to minimize vibrational noise at the microscope. The microscope mount assembly, designed with a two free-flex pivot, provides an angular degree of freedom for the alignment of the tip and sample with respect to the incoming X-ray beam. In this experiment, the sample was irradiated at a grazing angle of about 5°. The STM was operated in constant current mode with a loop gain of 3%. A detailed description of this SXSTM apparatus can be found elsewhere.[24]

Sample: A Cu(111) single crystal was cleaned in vacuum by several cycles of Ar^+ ion sputtering at temperatures between 300 and 900 K and subsequent annealing at 900 K using electron beam bombardment. The sample was slightly oxidized by the residual oxygen in the vacuum chamber.

Smart Tip: A SiO_2-coated $Pt_{90}Ir_{10}$ tip with sub-micron conducting apex was prepared by means of electron beam physical vapor deposition (EBPVD), focused ion beam milling and subsequent ion beam stimulated oxide growth.[20] Tips were electrochemically etched from a $Pt_{90}Ir_{10}$ wire with a diameter of 250 μm using a $CaCl_2$ solution. After cleaning with alcohol and H_2O, nominally 500 nm SiO_2 were deposited by EBPVD. In order to assure uniform coating the tips were mounted under an angle of about 17° with respect to the SiO_2 source and rotated at 20 rpm during deposition. A deposition rate of 0.1 nm/s was used at a base pressure of about 6×10^{-8} Torr. In order to remove oxide at the tip apex, FIB was utilized with Ga^+ ions impinging at the apex under normal incidence (30 kV, 50 pA). The exposed tip area was then minimized by the localized growth of an insulating film. For that purpose, a pentamethylcyclopentasiloxane precursor ($Si(OC_2H_5)_4$) was applied in situ through a nozzle in close proximity to the tip. The interactions of the precursor with the Ga^+ ions caused the deposition of an insulating film in areas where the ions were hitting the tip. After multiple iterations, which include rotation of the tip along the tip axis, an insulator coated tip with a sub-micron exposed apex was obtained.

Acknowledgements

This work was funded by the Office of Science Early Career Research Program through the Division of Scientific User Facilities, Office of Basic Energy Sciences of the U.S. Department of Energy through Grant SC70705. Work at the Advanced Photon Source, the Center for Nanoscale Materials, and the Electron Microscopy Center was supported by the U. S. Department of Energy, Office of Science, Office of Basic Energy Sciences, under contract DE-AC02-06CH11357.

Received: November 21, 2012
Revised: January 11, 2013
Published online: March 22, 2013

[1] D. Serrate, P. Ferriani, Y. Yoshida, S.-W. Hla, M. Menzel, K. von Bergmann, S. Heinze, A. Kubetzka, R. Wiesendanger, *Nat. Nanotechnol.* **2010**, *5*, 350.
[2] S.-W. Hla, *J. Vac. Sci. Technol., B* **2005**, *23*, 1351.
[3] R. Wiesendanger, M. Bode, R. Pascal, W. Allers, U. D. Schwarz, *J. Vac. Sci. Technol., A* **1996**, *14*, 1161.
[4] V. Rose, K. Brüggemann, R. David, R. Franchy, *Phys. Rev. Lett.* **2007**, *98*, 037202.
[5] T. A. Jung, F. J. Himpsel, R. R. Schlittler, J. K. Gimzewski, *Scanning Probe Microscopy: Analytical Methods* (Ed. R. Wiesendanger), Springer: Berlin, Germany **1998**, pp 11–48.
[6] V. Rose, J. W. Freeland, S. K. Streiffer, in: *Scanning Probe Microscopy of Functional Materials: Nanoscale Imaging and Spectroscopy* (Eds: S. V. Kalinin, A. Gruverman), Springer, New York, USA **2011**, p. 405.
[7] C.-Y. Chiu, Y.-L. Chan, Y. J. Hsu, D. H. Wie, *Appl. Phys. Lett.* **2008**, *92*, 103101.
[8] V. Rose, T. Y. Chien, J. W. Freeland, D. Rosenmann, J. Hiller, V. Metlushko, *J. Appl. Phys.* **2012**, *111*, 07E304.
[9] V. Rose, J. W. Freeland, *Proceedings of 2010 International Conference on Electromagnetics in Advanced Applications (ICEAA 2010)*, Sydney, Australia **2010**, pp. 201–204.
[10] K. Tsuji, K. Wagatsuma, K. Sugiyama, K. Hiraga, Y. Waseda, *Surf. Interface Anal.* **1999**, *27*, 132.
[11] T. Eguchi, T. Okuda, T. Matsushima, A. Kataoka, A. Harasawa, K. Akiyama, T. Kinoshita, Y. Hasegawa, M. Kawamori, Y. Haruyama, S. Matsui, *Appl. Phys. Lett.* **2006**, *89*, 243119.
[12] T. Scheler, M. Rodrigues, T. W. Cornelius, C. Mocuta, A. Malachias, R. Magalhaes-Paniago, F. Comin, J. Chevrier, T. H. Metzger, *Appl. Phys. Lett.* **2009**, *94*, 023109.
[13] V. Rose, J. W. Freeland, *AIP Conf. Proc.* **2010**, *1234*, 445.
[14] I. Schmid, J. Raabe, B. Sarafimov, C. Quitmann, S. Vranjkovic, Y. Pellmont, H. J. Hug, *Ultramicroscopy* **2010**, *110*, 1267.
[15] C. Fauquet, M. Dehlinger, F. Jandard, S. Ferrero, D. Pailharey, S. Larcheri, R. Graziola, J. Purans, A. Bjeoumikhov, A. Erko, I. Zizak, B. Dahmani, D. Tonneau, *Nano. Res. Lett.* **2011**, *6*, 308.
[16] A. Saito, J. Maruyama, K. Manabe, K. Kitamoto, K. Takahashi, K. Takami, M. Yabashi, Y. Tanaka, D. Miwa, M. Ishii, Y. Takagi, M. Akai-Kasaya, S. Shin, T. Ishikawa, Y. Kuwahara, M. Aono, *J. Synchrotron Rad.* **2006**, *13*, 216.
[17] T. Okuda, T. Eguchi, K. Akiyama, A. Harasawa, T. Kinoshita, Y. Hasegawa, M. Kawamori, Y. Haruyama, S. Matsui, *Phys. Rev. Lett.* **2009**, *102*, 105503.
[18] K. Akiyama, T. Eguchi, T. An, Y. Hasegawa, T. Okuda, A. Harasawa, T. Kinoshita, *Rev. Sci. Instrum.* **2005**, *76*, 083711.
[19] A. Saito, K. Takahashi, Y. Takagi, K. Nakamatsu, K. Hanai, Y. Tanaka, D. Miwa, M. Akaikasaya, S. Shin, S. Matsui, T. Ishikawa, Y. Kuwahara, M. Aono, *Surf. Sci.* **2007**, *601*, 5294.
[20] V. Rose, T. Y. Chien, J. Hiller, D. Rosenmann, R. P. Winarski, *Appl. Phys. Lett.* **2011**, *99*, 173102.
[21] M. Yin, C.-K. Wu, Y. Lou, C. Burda, J. T. Koberstein, Y. Zhu, S. O'Brien, *J. Am. Chem. Soc.* **2005**, *127*, 9506.
[22] V. Rose, J. W. Freeland, K. E. Gray, S. K. Streiffer, *Appl. Phys. Lett.* **2008**, *92*, 193510.
[23] J. W. Freeland, J. C. Lang, G. Srajer, R. Winarski, D. Shu, D. M. Mills, *Rev. Sci. Instrum.* **2002**, *73*, 1408.
[24] M. L. Cummings, T. Y. Chien, C. Preissner, V. Madhavan, D. Diesing, M. Bode, J. W. Freeland, V. Rose, *Ultramicroscopy* **2012**, *112*, 22.